*Article*

# Discrete Element Simulation of the Shear Behavior of Binary Mixtures Composed of Spherical and Cubic Particles

Yun Huang [1], Weichen Sun [2], Qiang Xie [2], Hongyi You [3] and Kai Wu [3,*]

[1] PowerChina Chengdu Engineering Corporation Limited, Chengdu 610000, China; huangyun@chidi.com.cn
[2] School of Civil Engineering, Chongqing University, Chongqing 400045, China; wcsun@cqu.edu.cn (W.S.);
xieqiang2000@163.com (Q.X.)
[3] School of Transportation, Southeast University, Nanjing 210096, China
* Correspondence: wukai2018@seu.edu.cn

**Abstract:** This research paper presents an investigation into the shear behavior of binary mixtures composed of cubic and spherical particles, employing the discrete element method (DEM) through triaxial tests simulations. A range of binary particle samples with varying volume fractions of cubic and spherical particles is generated for analysis. The study primarily focuses on examining the contracting-dilatancy relationship of binary granular material samples by scrutinizing deviatoric stress and volumetric strain curves, while considering the influence of confining pressure, initial porosity, and particle size ratio. Furthermore, the paper sheds light on the evolution of microstructures during the shearing process by presenting coordination numbers and rotational velocity fields for different particle types (overall particles, cubic particles, spherical particles), as well as between cubic-spherical particles. The findings demonstrate the substantial impact of both the volume fraction of cubic particles and the particle size ratio on the shear behavior of binary particles at both macroscopic and microscopic scales. Additionally, a comprehensive investigation reveals the dependence of anisotropy in normal contact forces, tangent contact forces, and contact orientations on the volume fraction of cubic particles.

**Keywords:** DEM; triaxial test; binary mixtures; particle shape; shear

## 1. Introduction

Granular materials have garnered significant attention as a distinct state of matter, finding wide-ranging applications in nature, everyday life, manufacturing, and technology. Examples include sand, soil, sugar, salt, and various industrial chemicals. The mechanical behavior of granular materials is influenced by multiple factors, such as particle size [1], particle shape [2], particle arrangement [3], and inter-particle friction [4]. However, due to the intricate interplay of these factors, isolating the specific impact of each one presents a challenge for researchers. To overcome this challenge, binary mixtures have emerged as a valuable approach for investigating the mechanical behavior of granular materials, wherein a specific influential factor is varied between two distinct states. By employing binary mixtures, researchers can effectively examine the isolated effects of individual factors, enabling a deeper understanding of granular material behavior.

Researchers have dedicated considerable efforts to investigating binary mixtures of granular materials using both experimental and numerical simulation approaches. Previous studies have highlighted the significant influence of volume fraction on the shear behavior of granular materials, wherein particle size heterogeneity affects packing density, shear strength, and energy dissipation. Moreover, the anisotropic fabric and stress tensors of granular media are directly related to integrated packing properties, which in turn, depend on particle size distribution. Additionally, it has been observed that fine and coarse particles play distinct roles in the formation of contact force chains. In the presence of coarse particles, fine particles dominate the contact force chains when in a floating state, whereas coarse

particles determine the force chain networks in a non-floating state. While existing studies have predominantly focused on the impact of particle size, limited research has explored the effects of particle shape. Notably, the shape of particles, whether non-spherical or spherical, has pronounced implications for the macro- and micro-mechanical properties of granular media. Non-spherical particles face greater resistance to rolling compared to spherical particles when subjected to forces and moments due to their shape barriers. Consequently, it is essential to investigate how particle shape influences the behavior of binary mixtures.

The discrete element method (DEM), proposed by Cundall and Strack [5], is a powerful tool for studying the mechanical behavior of granular materials [6–8]. The discrete element method offers advantages over the finite element method (FEM) in this topic, because FEM is a numerical simulation technique designed for continuous media. Specifically, when studying the physical and mechanical properties of granular media, the discrete element method proves to be more advantageous. DEM addresses individual particles and their interactions, making it ideal for studying granular media behavior [9]. DEM can capture the key response features of granular media at the macroscopic level, including those involved in large-displacement geomechanics problems, and can also be used to investigate microstructural changes such as contact force chains, displacement, and rotation field distribution, and coordination number fluctuation [10,11]. DEM has been used to simulate binary mixtures and to investigate the impact of particle shape. Non-spherical particles can be modeled using clump particles [12–15] or polygon particles [16–19]. The former modeling method uses multiple spherical particles to generate one clump particle, while the latter uses one spherical particle to create one polygon particle. In some cases, the rolling friction coefficient is used to reduce the rolling efficiency of spherical particles when modeling non-spherical particles [20–23]. The concept of polygon particles is simulated in the binary media to investigate the impact of particle shape on binary mixtures. Superellipsoid is a special polygon model for non-spherical particles that was first introduced by Williams et al. [24] and later extended to 3D by Cleary et al. [25]. It can describe 80% of solid shapes [26–29]. In this study, the cube, which is a unique shape of superellipsoid is used to characterize non-spherical particles.

The discrete element method (DEM), initially proposed by Cundall and Strack [5], has emerged as a powerful tool for investigating the mechanical behavior of granular materials [6–8]. The discrete element method offers several advantages over the finite element method, a numerical simulation technique designed for continuous media. Specifically, when studying the physical and mechanical properties of granular media, the discrete element method proves to be more advantageous [9]. At the macroscopic level, DEM can capture essential response features of granular media, including those relevant to large-displacement geomechanics problems. Furthermore, it enables the investigation of microstructural changes, such as contact force chains, displacement and rotation field distribution, and coordination number fluctuations [10,11]. DEM has been widely employed to simulate binary mixtures and explore the influence of particle shape. Non-spherical particles can be effectively modeled using clump particles, where multiple spherical particles combine to form a single clump particle [12–15]. Alternatively, polygon particles, where one spherical particle represents a polygon particle, have also been utilized [16–19]. In some cases, the rolling friction coefficient is adjusted to reduce the rolling efficiency of spherical particles when modeling non-spherical particles [20–23]. To investigate the impact of particle shape on binary mixtures, The concept of polygon particles, specifically employing the cube, a unique shape derived from the superellipsoid model introduced by Williams et al. [24] and extended to three dimensions by Cleary et al. [25] is adopted. The superellipsoid model has been demonstrated to accurately represent approximately 80% of solid shapes [26–29]. In this study, the cube, a distinctive superellipsoid shape, is utilized to characterize non-spherical particles within the binary media.

This study aims to explore the influence of the volume proportion of cubic to spherical particles on the shear behavior of binary mixtures, considering the impact of particle

shape. Binary samples comprising both spherical and cubic particles with varying volume fractions are prepared, and their shear strength and volumetric strain are analyzed from a macroscopic perspective. In addition to the macroscopic analysis, the microscopic metrics such as mechanical coordination number, contact force chains, and the anisotropy of normal and tangential forces are applied. These comprehensive analyses shed light on the underlying mechanisms governing the behavior of binary mixtures and provide valuable insights into the role of particle shape in shaping their macro and micromechanical properties.

## 2. Discrete Element Simulation

### 2.1. Contact Law

In this study, the PFC 3D software [30] (https://www.itascacg.com/software/PFC, accessed on 20 June 2023) is applied to perform discrete element method (DEM) simulations. The Hertz contact model is utilized as the contact law, which consists of a nonlinear Hertzian component based on the theory of Mindlin and Deresiewicz to calculate the normal forces [31]. The interaction force between two contacting particles is determined by their overlap, and a dissipative component is also incorporated.

The normal force can be calculated as follows

$$
F_n^h = \begin{cases} -h_n|g_c|^{\alpha_h} & ,g_c < 0.0 \\ 0.0 & ,otherwise. \end{cases} \tag{1}
$$

The coefficient $h_n$ depends on the geometrical and mechanical properties of the contacting pieces as

$$
h_n = \frac{2G\sqrt{2\bar{R}}}{3(1-\nu)} \tag{2}
$$

where $G$, $\nu$, and $\bar{R}$ are the effective shear modulus, Poisson's ratio, and contact radius, respectively. The effective shear modulus and Poisson's ratio can be input directly, or inherited from the contacting pieces as detailed below.

The effective radius of the contact is computed via the radii of the contacting piece surfaces as $\bar{R} = \dfrac{R_1 R_2}{2(R_1 + R_2)}$.

The tangential component $F_s$ is based on Coulomb's friction law, which is given by Equation (4) as follows:

$$
F_s^* = (F_s^h)_0 + k_s \Delta \delta_s \tag{3}
$$

where $(F_s^h)_0$ is the hertz shear force at the beginning of the timestep and $\Delta \delta_s$ is the relative shear increment. $k_s$ is the initial tangent shear stiffness, which depends on the current normal force as

$$
k_s = \frac{2(1-\nu)}{2-\nu} \alpha_h (h_n)^{1/\alpha_h} (F_n^h)^{(\alpha_h - 1)/\alpha_h} \tag{4}
$$

The value of $(F_s^h)_0$ depends on the scaling mode $M_s$:

$$
(F_s^h)_0 = \begin{cases} \dfrac{k_s}{(k_s)_0}(F_s^h)_0 & , \ if\, M_s = 1 \quad and \quad F_n^h < (F_n^h)_0 \\ (F_s^h)_0 & , \ otherwise. \end{cases} \tag{5}
$$

where $(F_n^h)_0$, $(F_s^h)_0$, and $(k_s)_0$ are the normal force, the shear force, and the tangent shear stiffness computed at the beginning of the timestep, respectively. $M_s = 1$ means that the shear-force scaling is active.

Compute the shear strength:

$$
F_s^\mu = \mu F_n^h \tag{6}
$$

The Hertz shear force is calculated as

$$F_s^h = \begin{cases} F_s^* & ,||F_s^*|| < F_s^\mu \\ F_s^\mu (F_s^*/||F_s^*||) & , \quad otherwise. \end{cases} \tag{7}$$

Update the slip state

$$s = \begin{cases} true & ,\left||F_s^h\right|| = F_s^\mu \\ false & , \quad otherwise. \end{cases} \tag{8}$$

If the slip state is true, then the contact is sliding. Whenever the slip states change, the slip change callback event occurs.

### 2.2. Generation of Cubic Particles

The cubic shape is in fact a variant of superellipsoid. The surface function of a super ellipsoidal particle in local Cartesian coordinates is defined in Equation (9):

$$\left(|\frac{x}{a}|^m + |\frac{y}{b}|^m\right)^{\frac{n}{m}} + |\frac{z}{c}|^n = 1.0 \tag{9}$$

where $x$, $y$, $z$ are the coordinates of a point on the surface of the superellipsoidal particle. The variables, $a$, $b$, $c$ denote the half-length of the particle along the principal axis of the local coordinate system of the superellipsoidal particle. The shape indexes $m$ and $n$ are two shape factors to determine the particle shape and the surface blockness. The shape index $m$ affects the upper and bottom margins, while the shape index $n$ controls the four side edges [32,33]. Simultaneous variation of $m$ and $n$ transforms the sphere into a cube. Keeping m constant, increasing n leads to sphere-to-cylinder conversion. Constant n and increased m yield walnut-like tetrahedron. m influences upper/lower surfaces, and n defines lateral shape. Cross-sectionally, augmented m shifts the upper surface from circular to square; increased n shifts the side from circular to square. Thus, simultaneous m and n increase results in sphere-to-cube transformation. Figure 1 shows the evolution path of superellipsoids from sphere to cube.
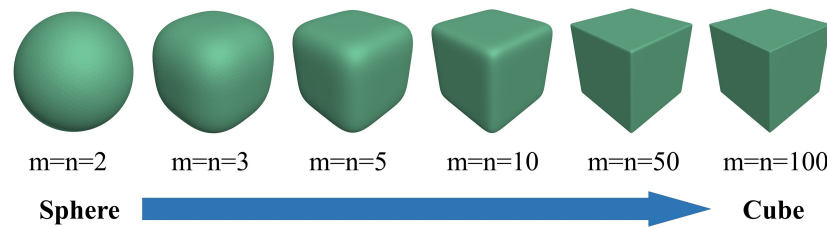


|          |          |          |           |           |            |
|----------|----------|----------|-----------|-----------|------------|
| m=n=2    | m=n=3    | m=n=5    | m=n=10    | m=n=50    | m=n=100    |

**Sphere** ⟶ **Cube**

**Figure 1.** Evolution of superellipsoids from sphere to cube by changing two shape factors $m$ and $n$ to determine the particle shape and the surface blockness.

### 2.3. DEM Simulation Procedure

The aim of this study is to investigate the shear strength of binary mixture samples using three-dimensional discrete element method (DEM) simulations of triaxial tests under the boundary condition of a rigid cylindrical wall in dry condition. The influence of water has not been considered in the simulations. The simulation procedure consists of three steps: sample generation, isotropic consolidation, and shearing process. Six binary mixture samples with different volume fractions of cubes and spheres, denoted as CxSy (where x and y represent the volume fraction of cubes and spheres, respectively) are examined. The samples under investigation are C100S0, C80S20, C60S40, C40S60, C20S80, and C0S100 (see Figure 2 for sample visualization). Each sample has a diameter of 50 mm and a height of 125 mm, with approximately 5000 particles of the equivalent diameter of 4 mm for both spherical and cubic particles. The L/D ratio of the sample is 2.5. The initial porosity of the

samples is approximately 0.45 monitored by measuring a circle in the middle of the sample. Default parameters for DEM simulations are employed (refer to Table 1 for specific DEM parameters). Following the sample generation, a stress servo-controlled rigid cylindrical wall boundary condition is applied to regulate the confining pressure throughout the isotropic consolidation and shearing stages. The servo-controlled boundary adjusts the radius of the rigid cylindrical wall in response to changes in lateral pressure, utilizing the Lame formula of Equation (10) [34] (see Figure 3) .
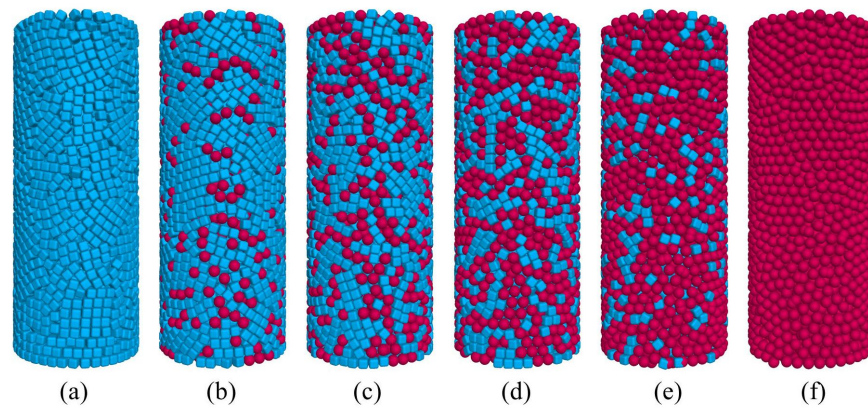


| (a) | (b) | (c) | (d) | (e) | (f) |

**Figure 2.** Mixture samples composed of varying volume fractions of spheres and cubes: (**a**) C100S0, (**b**) C80S20, (**c**) C60S40, (**d**) C40S60, (**e**) C20S80, (**f**) C0S100.

**Table 1.** Default parameters for DEM simulations of triaxial test on superellisoidal particles [35].

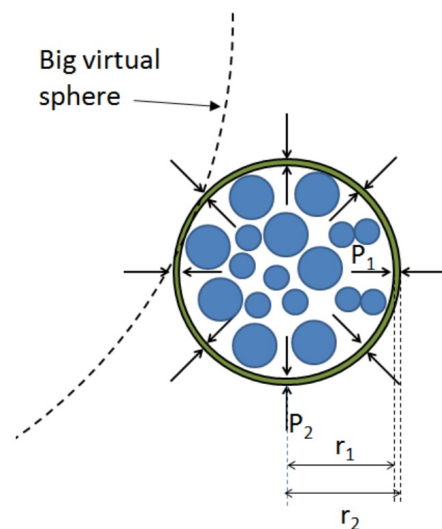| Parameter | Value | Unity |
|---|---|---|
| Shear modulus, $G$ | 650 | MPa |
| Poisson ratio, $v$ | 0.3 | |
| Exponent of hertz model, $\alpha_h$ | 1.5 | - |
| Local damping coefficient, $c$ | 0.7 | - |
| Density, $\rho$ | 2530 | kg/m$^3$ |
| Friction coefficient inter-particles, $\mu$ | 0.3 | - |
| Friction coefficient of wall-particles, $\mu_w$ | 0.0 | - |
| Confining pressure, $P_1$ | 1.0, 2.0 | MPa |



**Figure 3.** Cutting section of rigid cylinder boundary condition based on Lame formula [34].

$$\Delta r = \frac{1}{E}\left[\frac{(1-\nu)(r_1^2 P_1 - r_2^2 P_2)}{r_2^2 - r_1^2}r + \frac{(1+\nu)r_1^2 r_2^2 (P_1 - P_2)}{r_2^2 - r_1^2}\frac{1}{r}\right] \tag{10}$$

where $\Delta r$ is the radius variation, $E$ is Young's modulus of the cylinder, $r_1$ and $r_2$ are, respectively, the internal and external radius of cylindrical boundary condition, and $r$ is the radius between $r_1$ and $r_2$. The confining pressure $P_1$ is determined by dividing the total force exerted by the particles in contact with the cylinder boundary by the lateral surface area of the cylinder. To achieve the desired pressure, the servo-controlled rigid cylindrical boundary adjusts $P_1$ at each time step to match the target pressure $P_2$. The isotropic consolidation process is considered complete when $P_1$ reaches the target pressure $P_2$. During the shearing process, the confining pressure $P_1$ is maintained at a constant value while the servo-controlled cylindrical wall is adjusted. Simultaneously, the sample is subjected to compression by the upper and bottom platens. The shearing rate is controlled by the inertia number $I$ (Equation (11)), which determines the quasi-static state of the granular system [9].

$$I = \dot{\varepsilon}\sqrt{\frac{M}{P_1 d}} \tag{11}$$

where $\dot{\varepsilon}$ is the shear strain rate, $M$ and $d$ are the mass and diameter of the particle, and $P_1$ is the confining pressure. In our simulations, the shear strain rate is fixed at $1.0$ /s to maintain an inertia number $I$ below $10^{-3}$. This choice ensures that the granular system remains in a quasi-static state throughout the shearing process. The axial strain is continuously monitored to assess the progress of shearing. The simulation is concluded once the axial strain reaches a predetermined threshold of 30%.

The effective mean stress $p$ and the deviatoric stress $q$ are defined as follows:

$$p = (\sigma_1 + 2P_1)/3 \tag{12}$$

$$q = \sigma_1 - P_1 \tag{13}$$

where $\sigma_1$ denotes the axial stress obtained by dividing the applied force on the upper platen by the surface area of the upper platen.

The axial strain $\varepsilon_z$ and volumetric strain $\varepsilon_v$ are derived from the movements of rigid walls as follows:

$$\varepsilon_z = (h - h_0)/h_0 \tag{14}$$

$$\varepsilon_v = (v - v_0)/v_0 \tag{15}$$

where $h_0$ is the initial height of the sample, $h$ is the current height of the sample, $v_0$ is the initial volume of the sample, and $v$ is the current volume of the sample.

## 3. Macroscopic Behavior

### 3.1. Influence of Volume Fraction of Cubic Particles

Figures 4a and 5a illustrate the evolution of deviatoric stress as a function of axial strain for binary mixtures under different confinement conditions of 1.0 MPa and 2.0 MPa, respectively. The data exhibit a strain-softening behavior with increasing axial strain, which aligns with previous investigations on dense granular materials [36–38]. The porosity values of the sample vary from 0.44 to 0.51 during the simulation. Notably, when the volume fraction of cubes (FC) decreases from 100% to 80%, the deviatoric stress at the peak rises from 3.8 MPa to 4.2 MPa. However, as FC continues to decrease, the deviatoric stress at the peak decreases from 4.2 MPa to 3.9 MPa. For FC values below or equal to 60%, the deviatoric stress at an axial strain of 30% remains relatively constant. In contrast, the deviatoric stress at the residual state generally exhibits an increasing trend as FC increases. Consequently, the volume fraction of cubes significantly influences both the peak and critical-state shear strength of the mixtures. Furthermore, as the confining pressure

increases from 1.0 MPa to 2.0 MPa, the shear strength of granular mixtures nearly doubles. This finding underscores the substantial impact of confining pressure on the shear behavior of granular mixtures.
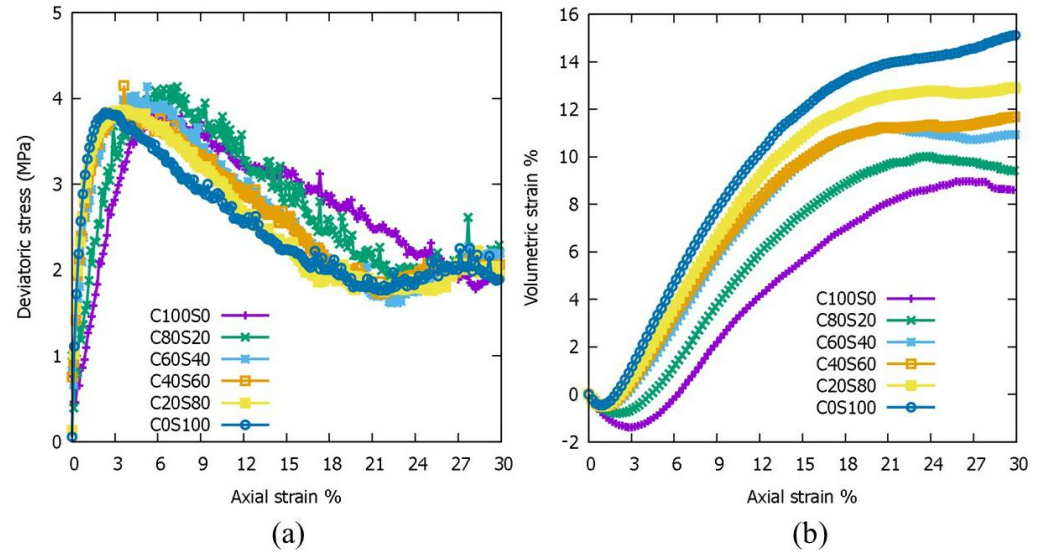


**Figure 4.** Comparisons of (**a**) deviatoric stress and (**b**) volumetric strain between different mixture samples under a confining pressure of 1.0 MPa.
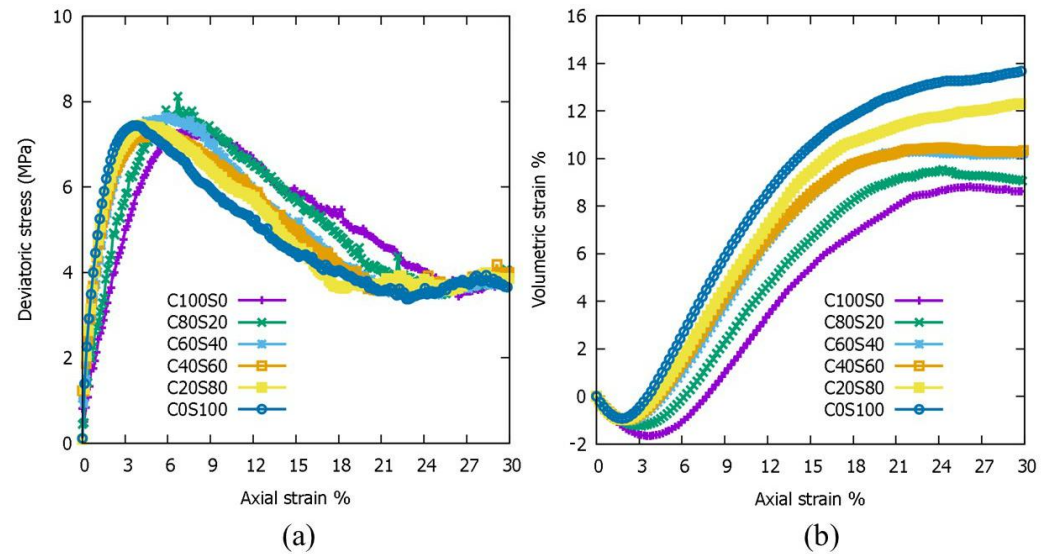


**Figure 5.** Comparisons of (**a**) deviatoric stress and (**b**) volumetric strain between different mixture samples under a confining pressure of 2.0 MPa.

Figures 4b and 5b present the evolution of volumetric strain as a function of axial strain for the binary mixtures subjected to confining pressures of 1.0 MPa and 2.0 MPa, respectively. Initially, the mixture samples undergo slight contraction followed by dilation. As the sample approaches the residual state, the slope of the volume strain curve gradually decreases, consistent with previous findings. This behavior can be attributed to the easier compaction of spherical particles, which necessitates more void space for shear, leading to enhanced dilation in granular systems with lower cubic particle content. Consequently, the volumetric strain of the sample increases as the volume fraction of spheres during shearing increases. Moreover, the confining pressure influences the volumetric strain response. Samples exhibit greater resistance to deformation and dilation under higher confining

pressures, as shown by the consistently higher volumetric strain under 1.0 MPa compared to that under 2.0 MPa.

The deviatoric stress and volumetric strain curves obtained from the triaxial shear test provide valuable insights into the intrinsic properties of granular materials, as demonstrated in Figure 6. These mechanical parameters, such as the friction angle ($\varphi$), dilatancy angle ($\psi$), Poisson's ratio ($\nu$), and stiffness modulus ($E$) offer further understanding of the shear behavior of granular media under specific test conditions.
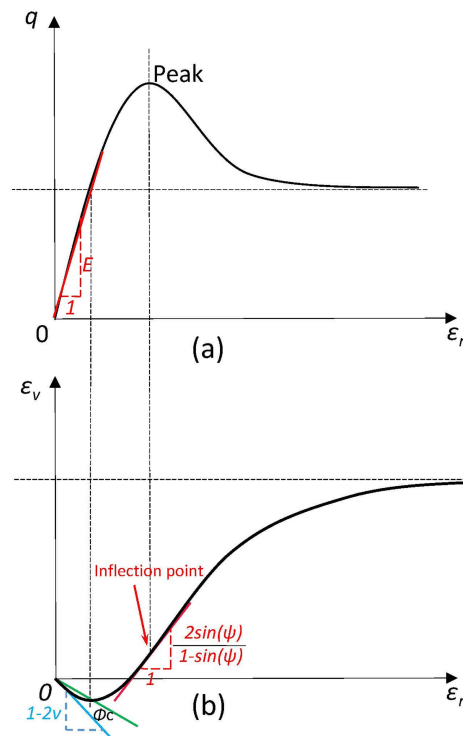


**Figure 6.** Mechanical parameters obtained from (**a**) deviatoric stress, and (**b**) volumetric strain curves under the triaxial shear test.

The friction angle $\varphi$ can be obtained from the deviatoric stress curve as a function of the effective stress ratio $M'$, Equations (16) and (17):

$$M' = q/p' \tag{16}$$

$$\varphi = \arcsin \frac{3M'}{M' + 6} \tag{17}$$

where $q$ denotes the deviatoric stress, $p'$ indicates the effective average stress and $M'$ denotes the effective stress ratio.

The dilatancy angle $\psi$ is determined by Equation (18) at an inflection point of the axial strain-volumetric strain curve as illustrated in Figure 6.

$$\psi = \arcsin \left( \frac{\frac{d\varepsilon_v}{d\varepsilon_r}}{2 + \frac{d\varepsilon_v}{d\varepsilon_r}} \right) \tag{18}$$

The relationship between the peak internal friction angle ($\sigma_{peak}$) and critical internal friction angle ($\sigma_{residual}$) with FC is depicted in Figure 7. As FC increases, the friction angles at peak initially increase until reaching 80%, after which they start to decrease. However, the friction angle at the residual stage consistently increases with FC, indicating that particle

shape has a greater influence on the strength of the granular material in the residual stage. Additionally, the dilatancy angle shows a decreasing trend as FC increases.
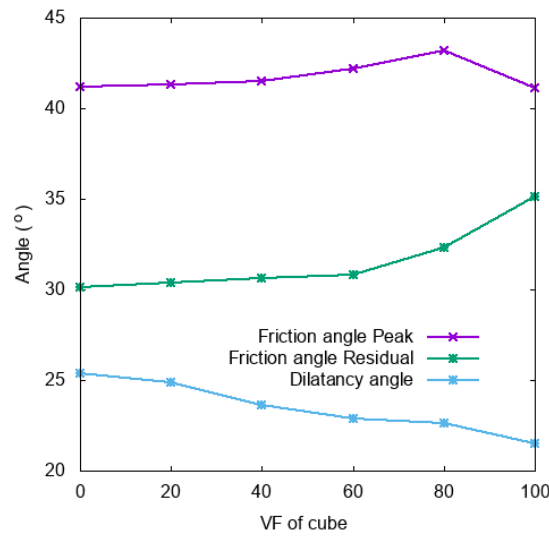


**Figure 7.** Evolution of friction angles at peak & residual stages and dilatancy angles as a function of volume fraction of cubic particles.

The elastic modulus (*E*) can be determined from the slope of the line between the point of 50% deviatoric stress and the origin. Figure 8a illustrates the variation of Young's modulus as a function of FC under confining pressures of 1.0 MPa and 2.0 MPa. It is evident that Young's modulus increases with FC, and it further increases with higher confining pressure. Poisson's ratio (*v*) measures the ratio of transverse to longitudinal strain resulting from a change in normal stress during compression. A value of 0.5 implies incompressibility, while a value of 0 indicates ease of compression. Poisson's ratio can be calculated using Equation (19). The variation of Poisson's ratio with FC under confining pressures of 1.0 MPa and 2.0 MPa is presented in Figure 8b. The Poisson's ratio increases with FC and also with an increase in confining pressure.
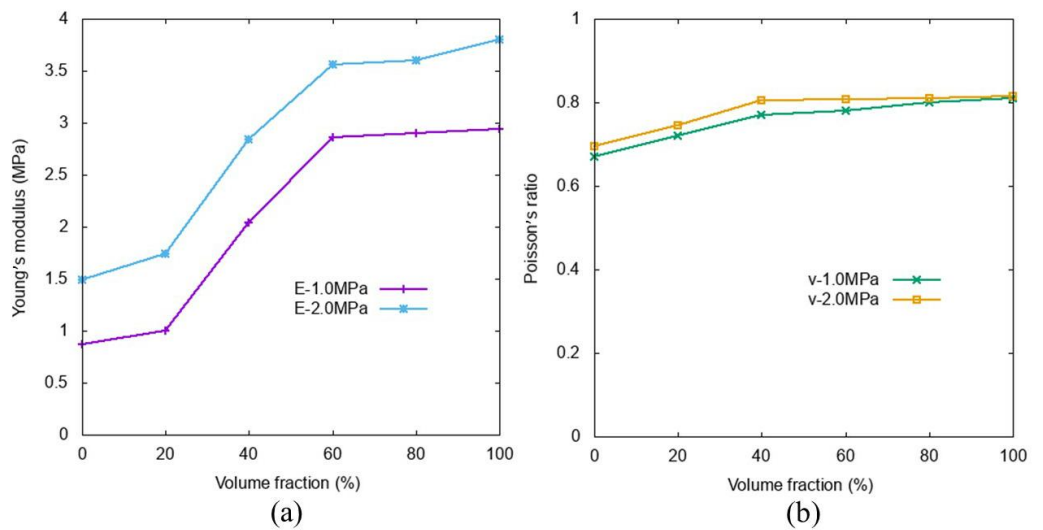


(a)



(b)

**Figure 8.** Comparisons of (**a**) Young's Modulus and (**b**) Poisson's ratio for different volume fraction mixture samples under confining pressures of 1.0 MPa and 2.0 MPa.

$$v = \frac{\varepsilon_a - \varepsilon_v}{2\varepsilon_a} \tag{19}$$

### 3.2. Influence of Initial Porosity

Figure 9 illustrates the comparison of simulation results for different initial porosities, highlighting the significant impact of initial porosity on the shear behavior of granular materials. A clear inverse correlation between shear strength and initial porosity is observed, indicating that an increase in initial porosity results in a decrease in the deviatoric stress at the peak. However, the effect of initial porosity on shear strength at the residual state is not evident, as the shear strength eventually converges as shearing progresses. Moreover, the volumetric strain shows an inverse relationship with initial porosity, where the dilatation of the sample volume weakens with increasing initial porosity.
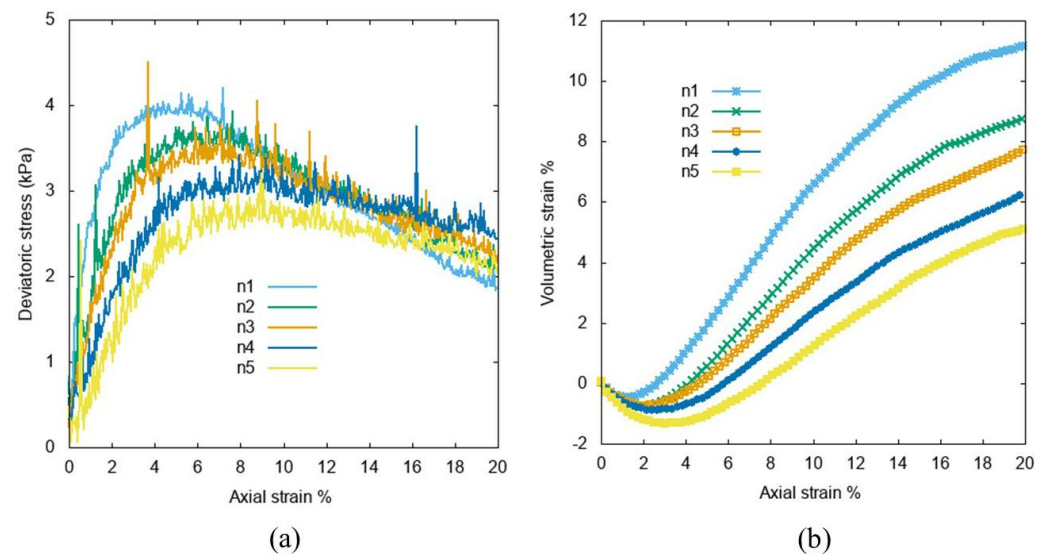


(a)  (b)

**Figure 9.** Influence of initial porosity on the (**a**) deviatoric stress and (**b**) volumetric strain for the mixture sample of C60S40 under the confining pressure of 1.0 MPa.

### 3.3. Influence of Particle Size Ratio

The influence of particle size ratio on the shear behavior of binary mixtures has received considerable attention in previous studies. However, there has been a noticeable gap in investigating the impact of particle shape on such behavior. To address this research gap, the effect of particle shape on the shear behavior of binary samples has been focused on, which consist of cubes and spheres with varying sizes. In this study, five mixtures are generated with a volume ratio of 1:1 for cubes and spheres, as outlined in Table 2. Sample SC represents a case where the particle sizes of cubes and spheres are equivalent. In Samples SS1 and SS2, the size of cubes is maintained while reducing the size of spheres. Conversely, for Samples SC1 and SC2, the size of spheres is kept constant while decreasing the size of cubes.

**Table 2.** Different particle sizes for mixture samples composed of cubes and spheres.

| ID | Cube Size | VF of Cube | No. of Cube | Sphere Size | VF of Sphere | No. of Sphere |
|---|---|---|---|---|---|---|
| SC | 4.0 mm | 50% | 2422 | 4.0 mm | 50% | 2381 |
| SS1 | 4.0 mm | 50% | 2398 | 3.0 mm | 50% | 5634 |
| SS2 | 4.0 mm | 50% | 2425 | 2.0 mm | 50% | 18,873 |
| SC1 | 3.0 mm | 50% | 5663 | 4.0 mm | 50% | 2381 |
| SC2 | 2.0 mm | 50% | 18,938 | 4.0 mm | 50% | 2381 |

Figure 10a presents the deviatoric stress profiles of the five prepared mixture samples. It is observed that the deviatoric stress decreases as the particle size decreases, irrespective of the particle shape. For example, when comparing samples SS1/SC1 or SS2/SC2 with

the same particle sizes, their peak strengths are nearly identical. However, the stress at the peak for samples SS1/SC1 is higher. Additionally, samples SC1 and SC2 exhibit a delayed attainment of peak strength compared to SS1 and SS2, indicating that smaller cube particle sizes result in a lower Young's modulus. Although the shear strengths of the five samples are almost identical at the residual state, suggesting that particle size has minimal effect on the residual state, the deviatoric stress curve exhibits the characteristic stick-slip phenomenon. This phenomenon can be attributed to variations in force networks under shear stress [39–42]. Previous studies have indicated that reducing the size of cube particles can amplify the amplitude of stick-slips.

Figure 10b presents the volumetric strain profiles of the five mixture samples with equivalent volume fractions of cubic and spherical particles but varying particle sizes under a confining pressure of 1.0 MPa. The results demonstrate that reducing the particle size has a substantial influence on sample expansion, as samples with smaller particle sizes display smaller expansions. This effect can be attributed to the ability of small particles to efficiently fill the void spaces between larger particles without significantly displacing the surrounding particles. Furthermore, it is observed that cubic particles exhibit less dilation compared to spherical particles of the same size. This behavior arises from the inherent characteristics of the particle shapes: spherical particles have a higher tendency to form dense packing structures, while cubic particles of the same volume exhibit a comparatively looser arrangement.
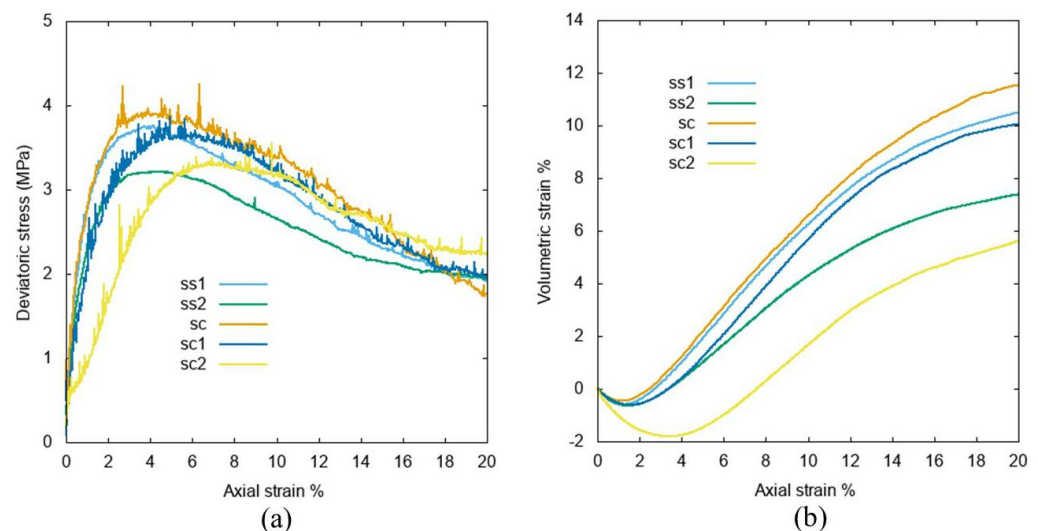


(a)



(b)

**Figure 10.** Comparisons of (**a**) deviatoric stress and (**b**) volumetric strain for mixture samples with different particle size ratios of cubes and spheres.

## 4. Microscopic Behavior

### 4.1. Coordination Number

The coordination number, defined by Equation (20), serves as a metric for quantifying the contact number of individual particles and provides insights into the packing density at the particle level [8,9,43].

$$Z = 2 \times \frac{C}{N} \tag{20}$$

where $Z$ is the coordination number, $C$ is the total contact number, and $N$ is the total particle number. However, it is worth noting that certain particles may have either no contact or only one contact with adjacent particles during the shearing process, rendering them less influential in maintaining a stable stress state. To address this issue, the mechanical average

coordination number, denoted as Zm, is introduced (as shown in Equation (21)), which excludes the contribution of these floating particles.

$$Z_m = \frac{2C - N_1}{N - N_0 - N_1} \qquad (21)$$

$$Z_{mc} = \frac{2C_c - N_{1c}}{N_c - N_{0c} - N_{1c}} \qquad (22)$$

$$Z_{ms} = \frac{2C_s - N_{1s}}{N_s - N_{0s} - N_{1s}} \qquad (23)$$

where $Z_m$ is the number of total particles, $Z_{mc}$ is the number of cubic particles, and $Z_{ms}$ is the number of spherical particles. $N_1$ and $N_0$ are the numbers of particles with only one or no contacts, and the subscripts $c$ and $s$ represent cubic and spherical particles, respectively.

Figure 11a presents the temporal evolution of the mechanical average coordination number, denoted as $Z_m$, for mixture samples with different volume fractions of cubic and spherical particles under a confining pressure of 1.0 MPa. The initial coordination number, $Z_m$, is relatively high and gradually decreases during the shearing process. Furthermore, it is observed that the coordination number, $Z_m$, decreases as the volume fraction of cubic particles increases. To further investigate the coordination number, Figure 11b showcases the evolution of the mechanical average coordination number, $Z_{mc}$, specifically between cubic particles, for samples with varying volume fractions of cubic particles under the confining pressure of 1.0 MPa. Interestingly, it is evident that $Z_{mc}$ decreases as the volume fraction of cubic particles decreases. In contrast, Figure 11c demonstrates the evolution of the mechanical average coordination number, $Z_{ms}$, specifically between spherical particles, under the confining pressure of 1.0 MPa. The results indicate that $Z_{ms}$ increases with a decrease in the volume fraction of cubic particles. Moreover, Figure 11d illustrates the evolution of the mechanical average coordination number, $Z_{msc}$, between cubic and spherical particles for samples with varying volume fractions of cubic particles under the confining pressure of 1.0 MPa. It is noteworthy that $Z_{msc}$ exhibits different initial values and initially increases, followed by a subsequent decrease as the volume fraction of cubic particles increases. This behavior arises due to the fact that the contact number between cubic and spherical particles is highest when the number of particles of both shapes is equal.

*4.2. Rotational Velocity Field*

The average rotational velocity is an important micromechanical metric for analyzing the mechanical behavior of binary mixture samples, and is defined as the average angular velocity of particles in a sample [43–45]. During shearing, the rotational velocity field of particles with different shapes is expected to differ. Figure 12 shows the variation of the average particle rotational velocity field for different mixture samples. The results indicate that the average particle rotational velocity increases as the FC decreases. Furthermore, Figure 13 depicts the rotational velocity of cubic and spherical particles during shearing. The rotational velocity of particles increases with the volume fraction of the corresponding particle shape. Previous studies [46,47] have suggested that particle rolling can offset the strengthening effect of inter-granular friction, while smaller particles tend to undermine the inter-particle locking effect due to their lubrication effect. In our study, cubic particles are demonstrated to tend to inhibit particle rotation.

The average rotational velocity serves as a crucial micromechanical parameter for analyzing the mechanical behavior of binary mixture samples, representing the average angular velocity of particles within a sample [43–45]. During shearing, it is expected that particles with different shapes will exhibit varying rotational velocity fields. Figure 12 presents the variation of the average particle rotational velocity field for different mixture samples. The results demonstrate that the average particle rotational velocity increases as the volume fraction of cubic particles decreases. Furthermore, Figure 13 displays the

rotational velocity of cubic and spherical particles during shearing. It is observed that the rotational velocity of particles escalates with an increase in the volume fraction of the corresponding particle shape. Notably, previous studies [46,47] have indicated that particle rolling can counterbalance the strengthening effect of inter-granular friction, whereas smaller particles tend to weaken the inter-particle locking effect due to their lubrication effect. In our study, cubic particles have been found to tend to impede particle rotation, supporting these prior findings.
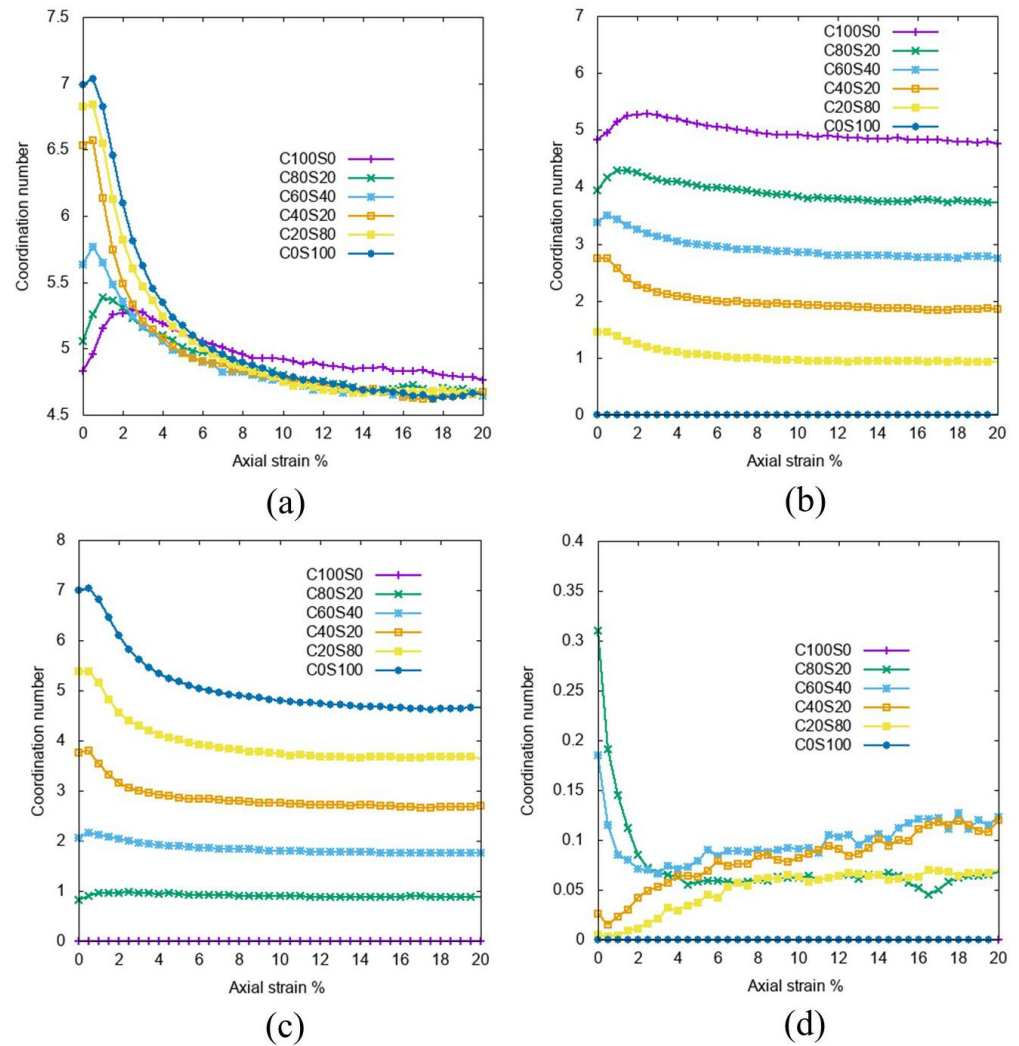


**Figure 11.** Evolution of mechanical average coordination number of (**a**) total particles $Z_m$, (**b**) cubic particles $Z_{mc}$, (**c**) spherical particles $Z_{ms}$, (**d**) cube-sphere particles $Z_{msc}$ for different mixture samples during the shearing stage.
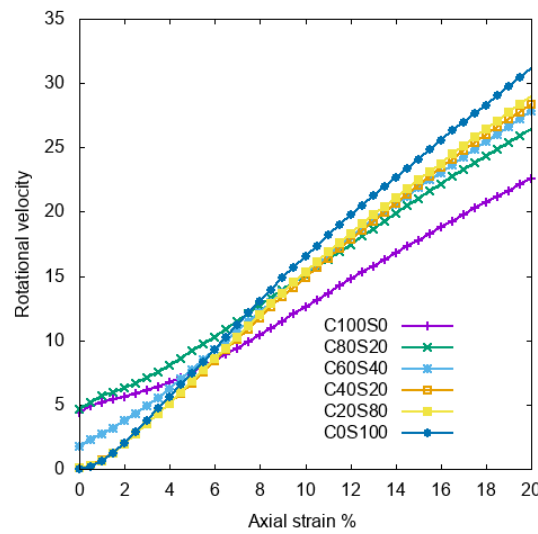
**Figure 12.** Evolution of average particle rotational velocity field for different mixture samples.
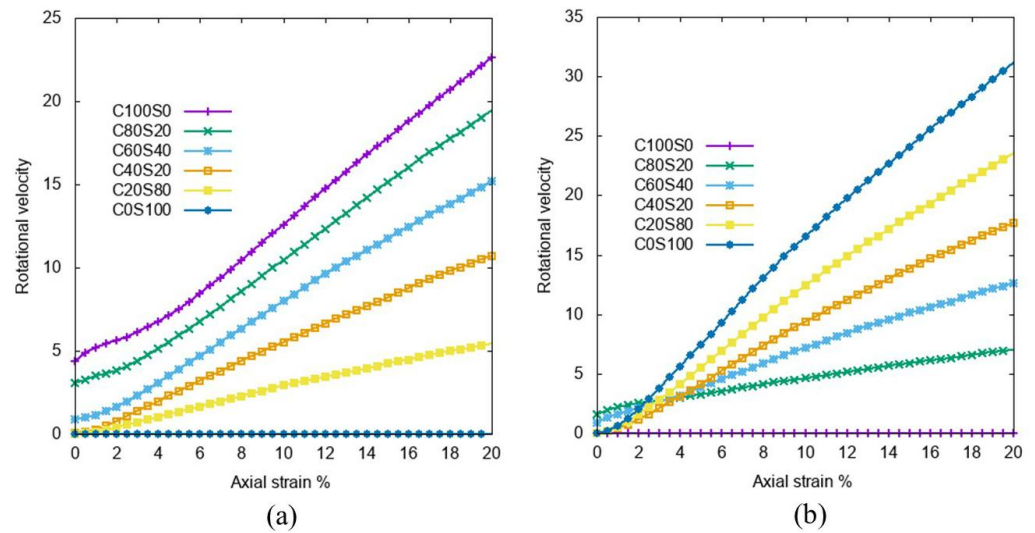


(a)　　　　　　　　　　　　　　　　(b)

**Figure 13.** Evolution of average particle rotation velocity of (**a**) cubic particles and (**b**) spherical particles for different mixture samples.

### 4.3. Contact Force Chains

Figure 14 illustrates the contact force chains in cubic-spherical mixture samples with varying volume fractions of each particle shape. Each force is represented by a color line connecting the particles in contact, with the color indicating the magnitude of the contact force. Strong forces are depicted in red, while weak forces are shown in blue. The results demonstrate that as the volume fraction of cubic particles increases, the strength of a single force chain intensifies, but the force chain network becomes more dispersed. Conversely, as the volume fraction of spherical particles increases, the strength of a single force chain diminishes, but the force chain network becomes more compact. These findings indicate that a decrease in the volume fraction of cubic particles leads to a decrease in the strength of individual force chains, while simultaneously increasing the density of the force chain network.
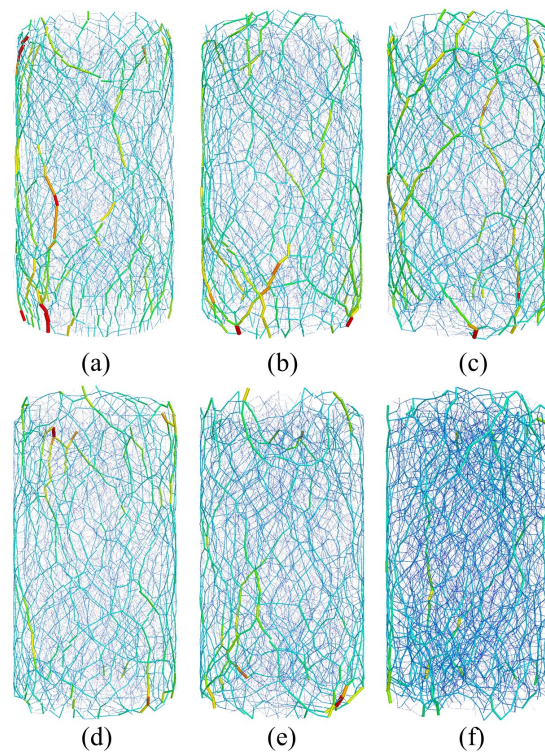
**Figure 14.** Contact force chains in different cubic-spherical mixture samples: (**a**) C100S0, (**b**) C80S20, (**c**) C60S40, (**d**) C40S60, (**e**) C20S80, (**f**) C0S100.

### 4.4. Fabric Anisotropy

The utilization of DEM simulation provides a significant advantage in examining the micro-mechanical behavior at the particle scale by capturing crucial microscopic parameters, including the anisotropy of normal and tangential forces, as well as contact orientations. Following the shearing process, the anisotropy of normal and tangential contact forces, along with contact orientations, was analyzed for mixture samples comprising cube-cube, cube-sphere, and sphere-sphere contacts. To visualize the spatial distribution of contacts, a 3D rose diagram was constructed based on the collected data, as shown in Figures 15–17. Each bar in the diagram represents the average contact number, average contact normal force, and average contact tangential force in the respective 3D direction. Figure 15 presents the anisotropy of normal stress among different contact types in the mixture samples. Although the anisotropy of normal stress gradually decreases with decreasing FC, the reduction is not significant. In contrast, the anisotropy of tangential stress increases as FC decreases, as depicted in Figure 16. The shape of the 3D rose contact diagram transitions from symmetrical cones to "X" shapes. Figure 17 showcases the anisotropy of contact orientations for mixture samples involving cube-cube, cube-sphere, and sphere-sphere contacts after shearing. The data indicates that contact orientations become more anisotropic when one particle type dominates the system, while they become more isotropic when the volume fractions of cubes and spheres are similar. The rose diagrams representing the anisotropy of these parameters offer valuable insights into the microscopic behavior of mixture samples.
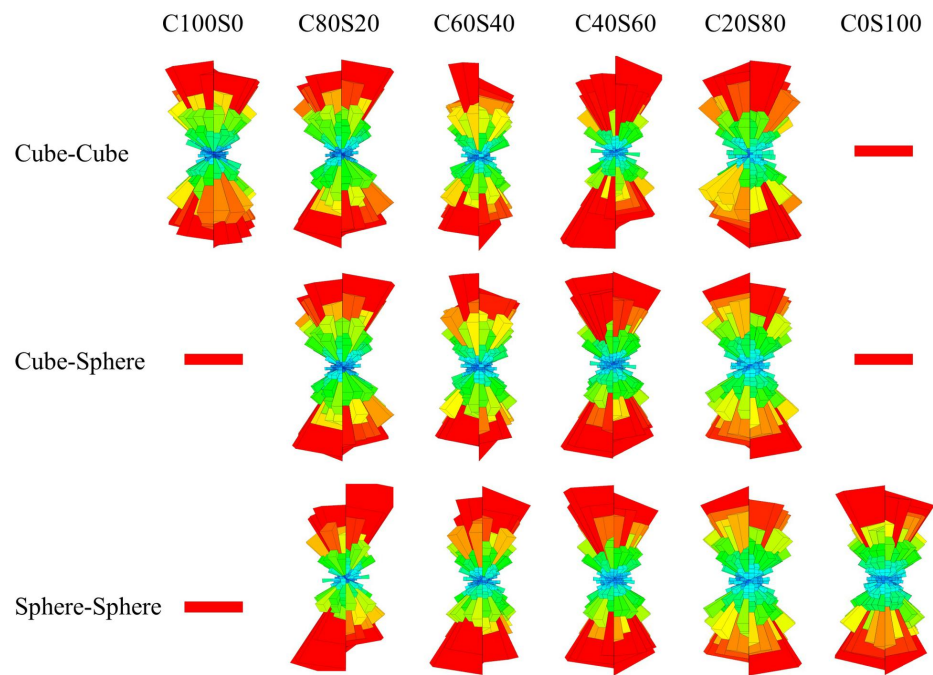
**Figure 15.** Anisotropy of normal contact forces for mixture samples between cube-cube, cube-sphere, and sphere-sphere after shearing.
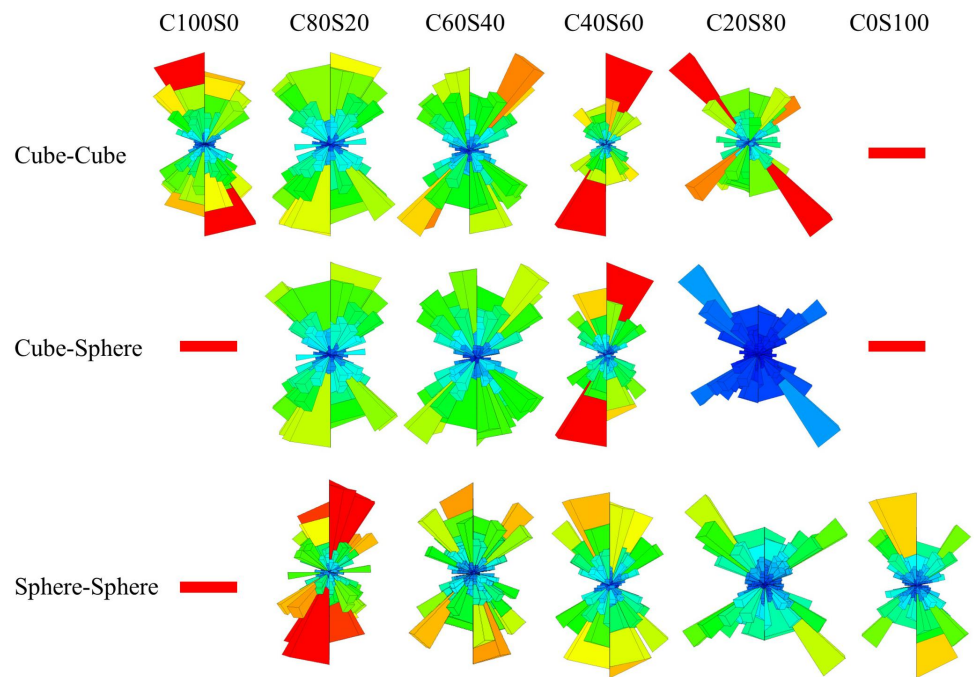


**Figure 16.** Anisotropy of tangent contact forces for mixture samples between cube-cube, cube-sphere, and sphere-sphere after shearing.
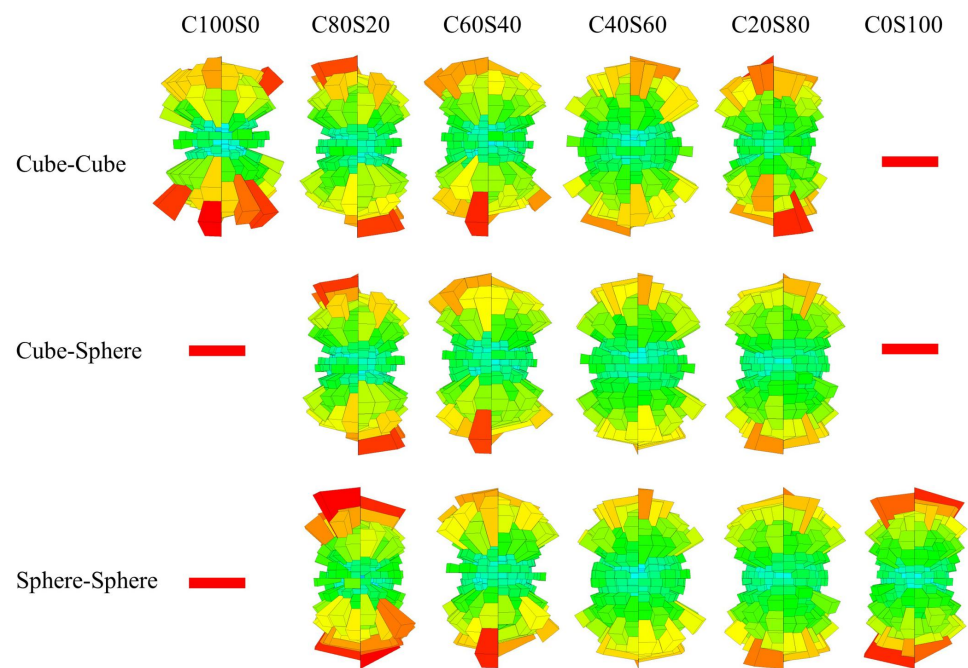
**Figure 17.** Anisotropy of contact orientations for mixture samples between cube-cube, cube-sphere, and sphere-sphere after shearing.

## 5. Conclusions

The primary aim of this study is to explore the shear behavior of binary mixture samples using DEM simulations of triaxial tests. These samples are composed of cubic and spherical particles with different volume fractions and particle size ratios. The investigation analyzes the mechanical characteristics of the binary mixture samples from both macroscopic and microscopic viewpoints. The obtained results yield several significant conclusions, which can be summarized as follows:

- The macroscopic shear behavior of binary particle samples is profoundly influenced by the volume fraction of cubic and spherical particles, as well as the particle size ratios. Variations in the volume fraction of these particles result in noticeable changes in deviatoric stress, volumetric deformation, as well as internal friction angles, dilatancy angles, stiffness modulus, and Poisson's ratio of the binary samples.
- From a microscopic standpoint, the analysis reveals the influence of particle characteristics on the coordination number of the individual particles. As the volume fraction of coarse particles increases, the overall coordination number of the system decreases. More specifically, the coordination number $Z_{mc}$ of cubic particles decreases as the volume fraction of spheres decreases. Conversely, the coordination number $Z_{ms}$ of spherical particles increases as the volume fraction of spheres decreases. These findings demonstrate the intricate relationship between particle characteristics and the coordination number at a microscopic level.
- The anisotropy of normal and tangential contact forces, as well as contact orientations, is influenced by the volume fraction of particles with different shapes. The variation in the volume fraction of particles with distinct shapes leads to changes in the directional distribution of contact forces and orientations.

**Author Contributions:** Methodology, investigation, original draft preparation, Y.H.; Software, Simulation, Data curation, W.S.; Validation, Supervision, Q.X.; Validation, H.Y.; Conception, Writing—review and editing, K.W. All authors have read and agreed to the published version of the manuscript.

**Institutional Review Board Statement:** Not applicable.

**Informed Consent Statement:** Not applicable.

**Data Availability Statement:** The data that support the findings of this study are available from the corresponding author upon reasonable request.

**Conflicts of Interest:** The authors declare no conflict of interest.

## References

1. Kumar, N.; Imole, O.I.; Magnanimo, V.; Luding, S. Effects of polydispersity on the micro-macro behavior of granular assemblies under different deformation paths. *Particuology* **2014**, *12*, 64–79. [CrossRef]
2. Yang, J.; Luo, X.D. Exploring the relationship between critical state and particle shape for granular materials. *J. Mech. Phys. Solids* **2015**, *84*, 196–213.
3. Wiacek, J.; Molenda, M. Effect of particle polydispersity on micromechanical properties and energy dissipation in granular mixtures. *Particuology* **2014**, *16*, 91–99.
4. Cheung, G.; O'Sullivan, C. Effective simulation of flexible lateral boundaries in two- and three- dimensional DEM simulations. *Particuology* **2008**, *6*, 483–500. [CrossRef]
5. Cundall, P.A.; Strack, O.D.L. A discrete numerical model for granular assemblies. *Geotechnique* **1979**, *29*, 47–65. [CrossRef]
6. Cho, G.C.; Dodds, J.; Santamarina, J.C. Particle shape effects on packing density, stiffness and strength: natural and crushed sands. *J. Geotech. Geoenviron. Eng.* **2006**, *132*, 591–602.
7. Yang, J.; Wei, L.M. Collapse of loose sand with the addition of fines: The role of particle shape. *Geotechnique* **2012**, *62*, 1111–1125.
8. Gu, X.Q.; Yang, J. A discrete element analysis of elastic properties of granular materials. *Granul. Matter* **2013**, *15*, 139–147. [CrossRef]
9. O'Sullivan, C. *Particulate Discrete Element Modelling*; CRC Press: Boca Raton, FL, USA, 2011.
10. Feng, Y.T. An energy-conserving contact theory for discrete element modelling of arbitrarily shaped particles: Basic framework and general contact model. *Comput. Methods Appl. Mech. Eng.* **2021**, *373*, 113454.
11. Hu, J.Y.; Ma, T.; Ma, K. DEM-CFD simulation on clogging and degradation of air voids in double-layer porous asphalt pavement under rainfall. *J. Hydrol.* **2021**, *595*, 126028.
12. Kodicherla, S.P.K.; Gong, G.B.; Yang, Z.X.; Krabbenhoft, K.; Fan, L.; Moy, C.K.S.; Wilkinson, S. The influence of particle elongations on direct shear behaviour of granular materials using DEM. *Granul. Matter* **2019**, *21*, 86.
13. Qian, Q.; An, X.Z.; Zhao, H.Y.; Dong, K.J.; Yang, X.H. Numerical investigations on random close packings of cylindrical particles with different aspect ratios. *Powder Technol.* **2019**, *343*, 79–86.
14. Jiang, M.J.; Zhang, A.; Fu, C. 3-D DEM simulations of drained triaxial tests on inherently anisotropic granulates. *Eur. J. Environ. Civ. Eng.* **2017**, *22*, 37–56.
15. Salimi, M.J.; Lashkari, A. Undrained true triaxial response of initially anisotropic particulate assemblies using CFM-DEM. *Comput. Geotech.* **2020**, *124*, 103509.
16. Cleary, P.W. DEM prediction of industrial and geophysical particle flows. *Particuology* **2010**, *8*, 106–118.
17. Wellmann, C.; Lillie, C.; Wriggers, P. Comparison of the macroscopic behavior of granular materials modeled by different constitutive equations on the microscale. *Finite Elem. Anal. Des.* **2008**, *44*, 259–271.
18. Zhao, S.; Zhou, X.; Liu, W. Discrete element simulations of direct shear tests with particle angularity effect. *Granul. Matter* **2015**, *17*, 793–806.
19. Boton, M.; Azema, E.; Estrada, N.; Radja, F.; Lizcano, A. Quasistatic rheology and microstructural description of sheared granular materials composed of platy particles. *Phys. Rev. E* **2013**, *87*, 032206.
20. Iwashita, K.; Oda, M. Rolling Resistance at Contacts in Simulation of Shear Band Development by DEM. *J. Eng. Mech.* **1998**, *124*, 285–292.
21. Ai, J.; Chen, J.F.; Rotter, J.M.; Ooi, J.Y. Assessment of rolling resistance models in discrete element simulations. *Powder Technol.* **2011**, *206*, 269–282.
22. Wu, W.; Ma, G.; Zhou, W.; Wang, D.; Chang, X.L. Force transmission and anisotropic characteristics of sheared granular materials with rolling resistance. *Granul. Matter* **2019**, *21*, 88.
23. Xie, C.H.; Ma, H.Q.; Zhao, Y.Z. Investigation of modeling non-spherical particles by using spherical discrete element model with rolling friction. *Eng. Anal. Bound. Elem.* **2019**, *105*, 207–220.
24. Williams, J.R.; Pentland, A.P. Superquadrics and model dynamics for discrete elements in interactive design. *Eng. Comput.* **1992**, *9*, 115–127.
25. Cleary, P.; Ha, J. Large scale industrial DEM modeling. *Eng. Comput.* **2000**, *21*, 169–204. [CrossRef]
26. Xie, C.H.; Song, T.; Zhao, Y.Z. Discrete element modling and simulation of non-spherical particles using polyhedrons and super-ellipsoids. *Powder Technol.* **2020**, *368*, 253–267. [CrossRef]

27. Zhao, Y.Z.; Xu, L.; Umbanhowar, P.B.; Lueptow, R.M. Discrete element simulation of cylindrical particles using super-ellipsoids. *Particuology* **2019**, *46*, 55–66.

28. Liu, J.Y.; Nicot, F.; Zhou, W. Sustainability of internal structures during shear band forming in 2D granular materials. *Powder Technol.* **2018**, *338*, 458–470.

29. Zhong, W.; Yu, A.; Liu, X.; Tong, Z.; Zhang, H. DEM/CFD-DEM modelling of non-spherical particulate systems: theoretical developments and applications. *Powder Technol.* **2016**, *302*, 108–152.

30. Itasca. *PFC 5.0 Documentation, PFC3D (Particle Flow Code in 3 Dimensions)*, version 5.0, user's manual; Itasca: Minneapolis, MN, USA, 2016.

31. Wu, K.; Remond, S.; Abriak, N.E.; Pizette, P.; Becquart, F.; Liu, S.Y. Study of the shear behavior of binary granular materials by DEM simulations and experimental triaxial tests. *Adv. Powder Technol.* **2017**, *28*, 2198–2210.

32. Li, C.X.; Zhou, Z.Y.; Zou, R.P.; Pinson, D.; Shen, Y.S.; Yu, A.B. Experimental and numerical investigation on the packing of binary mixtures of spheres and ellipsoids. *Powder Technol.* **2020**, *360*, 1210–1219.

33. Ji, S.Y.; Wang, S.Q.; Zhou, Z.Y. Influence of particle shape on mixing rate in rotating drums based on super-quadric DEM simulations. *Adv. Powder Technol.* **2020**, *31*, 3540–3550.

34. Wu, K.; Pizette, P.; Becquart, F.; Remond, S.; Abriak, N.E.; Xu, W.Y.; Liu, S.Y. Experimental and numerical study of cylindrical triaxial test on mono-sized glass beads under quasi-static loading condition. *Adv. Powder Technol.* **2017**, *28*, 155–166.

35. Wu, K.; Sun, W.C.; Liu, S.Y.; Cai., G.J. Influence of particle shape on the shear behavior of superellipsoids by discrete element method in 3D. *Adv. Powder Technol.* **2021**, *32*, 4017–4029.

36. Tang, H.X.; Zhang, X.; Ji, S.Y. Discrete Element Analysis for Shear Band Modes of Granular Materials in Triaxial Tests. *Part. Sci. Technol. Int. J.* **2016**, *35*, 277–290.

37. Wang, D.; Zheng, H.; Ji, Y.; Bares, J.; Behringer, R.P. Shear of granular materials composed of ellipses. *Granul. Matter* **2020**, *22*, 5.

38. Fazekas, S.; Torok, J.; Kertesz, J. Critical packing in granular shear bands. *Phys. Rev. E* **2007**, *75*, 011302.

39. Cui, D.S.; Wu, W.; Xiang, W.; Doanh, T.; Chen, Q.; Wang, S.; Liu, Q.B.; Wang, J.G. Stick-slip behaviours of dry glass beads in triaxial compression. *Granul. Matter* **2017**, *19*, 1.

40. Adjemian, F.; Evesque, P. Experimental study of stick-slip behaviour. *Int. J. Numer. Anal. Geomech.* **2004**, *28*, 501–530. [CrossRef]

41. Alshibli, K.A.; Roussel, L.E. Experimental investigation of slip-stick behaviour in granular materials. *Int. J. Numer. Anal. Meth. Geomech.* **2006**, *30*, 1391–1407.

42. Ozbay, A.; Cabalar, A.F. Effects of triaxial confining pressure and strain rate on stick-slip behavior of a dry granular material. *Granul. Matter* **2016**, *16*, 60.

43. Gu, X.Q.; Huang, M.S.; Qian, J.G. Discrete element modeling of shear band in granular materials. *Theor. Appl. Fract. Mech.* **2014**, *72*, 37–49. [CrossRef]

44. Iwashita, K.; Oda, M. Micro-deformation mechanism of shear banding process based on modified distinct element method. *Powder Technol.* **2000**, *109*, 192–205. [CrossRef]

45. Jiang, M.J.; Chen, H.; Tapias, M.; Arroyo, M.; Fang, R. Study of mechanical behavior and strain localization of methane hydrate bearing sediments with different saturations by a new DEM model. *Comput. Geotech.* **2014**, *57*, 122–138. [CrossRef]

46. Oda, M.; Iwashita, K.; Kakiuchi, T. Importance of particle rotation in the mechanics of granular materials. *Powders Grains* **1997**, *97*, 207–210.

47. Zhou, W.; Xu, K.; Ma, G.; Yang, L.F.; Chang, X.L. Effects of particle size ratio on the macro- and microscopic behaviors of binary mixtures at the maximum packing efficiency state. *Granul. Matter* **2016**, *18*, 81.